ACS APPLIED MATERIALS & INTERFACES

Research Article

www.acsami.org

Amine-Rich Polyelectrolyte Multilayers for Patterned Surface Fixation of Nanostructures

Stefan V. Stoianov,[†] Chalongrat Daengngam,[†] Malihe Borhani,[†] Yafen Zhang,[‡] John R. Morris,[‡] and Hans D. Robinson*,[†]

[†]Department of Physics and [‡]Department of Chemistry, Virginia Tech, Blacksburg, Virginia 24061, United States

ABSTRACT: We describe a lithographic method for directly patterning the adhesive properties of amine-rich layer-by-layer assembled polymer films, useful for positioning metal and other nanostructures. The adhesive properties of the films are sufficiently robust that the films can be patterned with standard as opposed to soft lithographic methods. We perform the patterning with a lithographically defined evaporated aluminum mask which protects selected regions of the substrate, passivating adhesion in the exposed regions with acetic anhydride. When the aluminum is removed with a HCl etch, the protected regions retain their adhesion, whereas particle adsorption is almost completely eliminated in the passivated areas, making it possible to guide adsorption to the protected areas. The high degree of adhesion comes about because of uncoordinated amine groups that pervade the film. Cycling the pH from high values to low and back causes the amines to be rearranged, rejuvenating the adhesive properties of the surface, which is the likely origin of the robustness of the adhesive properties to processing. pH adjustment also causes reversible swelling and deswelling of the film, so that the vertical position and dielectric environment of the nanostructure can be dynamically adjusted, which can be particularly beneficial for tuning the plasmonic resonances of metallic structures.

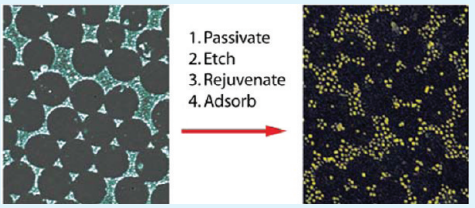

KEYWORDS: *polyelectrolyte multilayer, adhesion, lithography, surface assembly, plasmonics, surface rejuvenation*

INTRODUCTION

Full realization of all the promises of nanotechnology will require merging top-down and bottom-up fabrication technologies. For instance, accurate spatial positioning of bottom-up fabricated nanoparticles[1] and nanoassemblies[2−5] provided by top-down lithographic methods will become necessary in all but the simplest devices and systems. A similar interest in controlling the positioning of living cells exists for applications such as tissue engineering, biosensors and cellular studies.[6] Both cells and nanostructures are generally quite fragile and typically cannot withstand the processing conditions of most forms of lithography. This limitation can be overcome by instead patterning the adhesive properties of a substrate, so that adsorption of nano- or biostructures at desired locations can be the very last step in the fabrication process.

As the adhesive properties of a surface are themselves quite sensitive, creating patterns of adhesion is a nontrivial task.[6] One method to accomplish this is to use standard lithographic processing to prepattern the surface with materials (e.g., gold), that can be thoroughly cleaned and functionalized orthogonally from a glass or silicon substrate to selectively bind desired structures.[7] Lift-off of layer-by-layer (LbL)[8] or spun-on[9] films are other ways to achieve the same goal. Soft lithography techniques such as microcontact printing,[10−12] dip-pen nanolithography,[13] or microfluidic patterning[14] are quite popular. Other techniques to create surface patterns of particles or cells include electrostatic patterning,[15] dielectrophoresis,[16] and even patterning with magnetic fields.[17]

Here, we pattern the adhesive properties of ionic polyelectrolyte multilayer (PEM) films, also known as ionic self-assembled multilayer (ISAM) films[18−20] that are rich in amine groups, a property that makes them strongly adhesive to a variety of nanostructures. Previous work on patterning PEMs have typically employed either microcontact printing techniques[12,21−23] or selective deposition on a prepatterned surface.[24,25] Here, we show that the adhesive properties of amine-rich PEMs are sufficiently robust that they can be patterned by a much harsher technique; using an evaporated metal mask to protect the surface from chemical passivation with acetic anhydride, followed by removal of the mask by wet-etching. The significance of this is that standard lithographic techniques, normally used in semiconductor device processing, can in fact be used directly to pattern the adhesive properties of a substrate. This has the potential to facilitate the practical integration of bottom-up and top-down fabrication techniques.

The lithographic process is illustrated in Figure 1. First, an amine-rich PEM film is deposited on the charged substrate (Figure 1a). An aluminum mask is patterned on the film (Figure 1b), and the adhesive properties of the exposed film are passivated by immersing the substrate in acetic anhydride, which acetylates the free amine groups in the film, lowers the surface energy and reduces the number of sites available for hydrogen bonding, thereby reducing surface adhesion in those

Received: May 22, 2011
Accepted: April 4, 2012
Published: April 4, 2012

   dx.doi.org/10.1021/am300117f | ACS Appl. Mater. Interfaces 2012, 4, 2348−2357

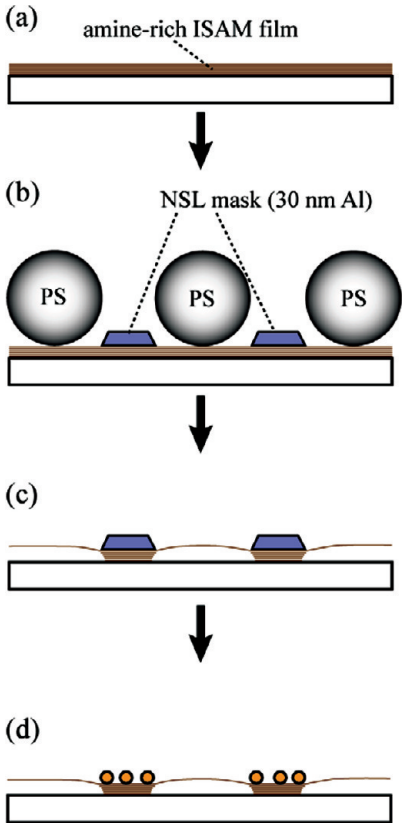

Figure 1. Schematic of the adhesion patterning process. (a) An amine-rich PEM film is deposited on the substrate. (b) A metal (Al) mask is deposited on the PEM film with nanosphere lithography. (c) The adhesion to the surface is passivated with acetic anhydride. The mask remains securely attached. (d) The mask is removed with wet-etching, and nanostructures can be preferentially adhered to the exposed areas.

areas not covered by metal (Figure 1c). The metal mask is then etched away, and other structures, proteins or compounds can be adsorbed onto the substrate. (Figure 1d). A very high contrast is seen between unmodified areas (where particles adhere strongly) and passivated areas (where very little particle adhesion is observed).

The process allows lithographic features to be created with a resolution better than 100 nm, and there is no reason to believe the ultimate limit should be any worse than what can be obtained with microimprint lithography. The process works better and is more robust the higher the amine content of the films, and we conclude that it is indeed the amines that are responsible for the good adhesion we observe. We believe the robustness stems from the fact that most of the amine groups in the film are coiled up into hydrophobic regions, buried in the bulk of the film, or both. The amines can be rearranged by modulating the film pH, which leads to at least a partial rejuvenation of the film, removing or neutralizing damage and fouling in a way that is not available, for example, in a silane monolayer. This hypothesis is supported by our observation that an amine-rich PEM film that is terminated with layer of polyanions will not adsorb negatively charged particles when first fabricated, but will readily do so after the pH has been cycled from alkaline to acidic and back.

This type of adhesion layer is particularly useful in plasmonic applications, as it does not degrade the plasmonic properties of surface-bound metal structures. An example of such applications include colloidal gold plasmonic sensors,[26−29] which can be used to detect the presence of an analyte that shifts the plasmon resonance of the particles when it binds to them. Another example is surface enhanced Raman spectroscopy (SERS),[30−32] which makes it possible to measure the Raman spectrum of minute quantities of a molecule, even as small as a single substance.[31,32] Both these techniques rely on strong plasmon resonances, which means that conventional gold and silver adhesion layers, made from metals such as Cr, Ni, or Ti are not useful, as they tend to strongly degrade the plasmon resonances.[33,34] As the films we use are entirely dielectric, this problem is avoided.

Another advantage of our approach is that it makes self-aligning adhesion lithography possible. Specifically, one can adsorb one type of nanoparticle on the surface and then passivate the adhesion to the film, taking the process through the stage shown in Figure 1c. The particles will remain securely attached, since the film below them is masked from the passivation. However, particles and compounds introduced later will not bind to the passivated areas of the surface, which makes it possible to modify and add to the bound nanostructures through self-assembly[35] without having to take additional precautions to avoid nonspecific binding elsewhere on the surface.

MATERIALS AND METHODS

Precleaned glass slides, acetic anhydride, sodium hydroxide, and hydrochloric acid were purchased from Fisher Scientific. Poly (allylamine hydrochloride) (PAH) M_W = 15,000, Poly (sodium 4-styrene-sulfonate) (PSS) M_W = 1 000 000, sodium citrate, gold(III)-chloride trihydrate, and other chemicals were obtained from Sigma Aldrich. GoldSeal UltraStick APTES terminated slides were purchased from Electron Microscopy Sciences. 99.999% gold and 99.99% Aluminum for evaporation were purchased from International Advanced Materials and Kurt J. Lesker, respectively. The PEM films were deposited on standard precleaned 1 in. × 3 in. microscope slides, which were first cleaned by immersion in a 1:4:20 solution of NH_4OH:H_2O_2:H_2O at 80 ± 5 °C for 15 min, followed by a 1:1:5 solution of HCl:H_2O_2:H_2O at 80 ± 5 °C for an additional 15 min. Between and after the immersion steps, the slides were rinsed with copious amounts of DI water and then stored in nanopure water until used.

PEM Deposition, Swelling, and Passivation. PEM films were deposited on the cleaned slides. The deposition was done by consecutively dipping each slide in aqueous solutions of PAH and PSS for 45s, with thorough rinsing in DI water between each step. The water and polyelectrolyte solutions were all adjusted to the same initial pH, which ranged from 6.5 to 9.5. The concentration of the polyelectrolyte solutions were 10 mM on a monomer basis. The pH of the solutions and rinsewater were adjusted and monitored to not deviate more than ±0.02 pH units during the deposition process. Between 1 and 10 bilayers of PAH/PSS were deposited and capped with a final layer of PAH. Such a film containing n bilayers plus a PAH layer will be denoted $(PAH/PSS)_n/PAH$, whereas those terminated with PSS will be denoted $(PAH/PSS)_n$.

The films were swelled by soaking them for 10 min in DI water adjusted with HCl to pH 3.25, and deswelled by a 30 min soak in DI water adjusted with NaOH to pH 10.25. After swelling and/or dewelling, the substrates were rinsed with DI water (pH ∼5.5) and used immediately.

Surface amines were passivated by acetylation with acetic anhydride. The substrates were first dried in a convection oven at 115 °C, and then immersed in neat acetic anhydride (97%+, Acros Organic) for 20 min. They were then soaked in methanol for a few minutes before being thoroughly rinsed in methanol followed by DI water. The 20 min treatment time is not critical; 5 or 10 min already leads to a good passivation, whereas immersion in acetic anhydride for as long as 2 h will not visibly damage or dissolve the film.

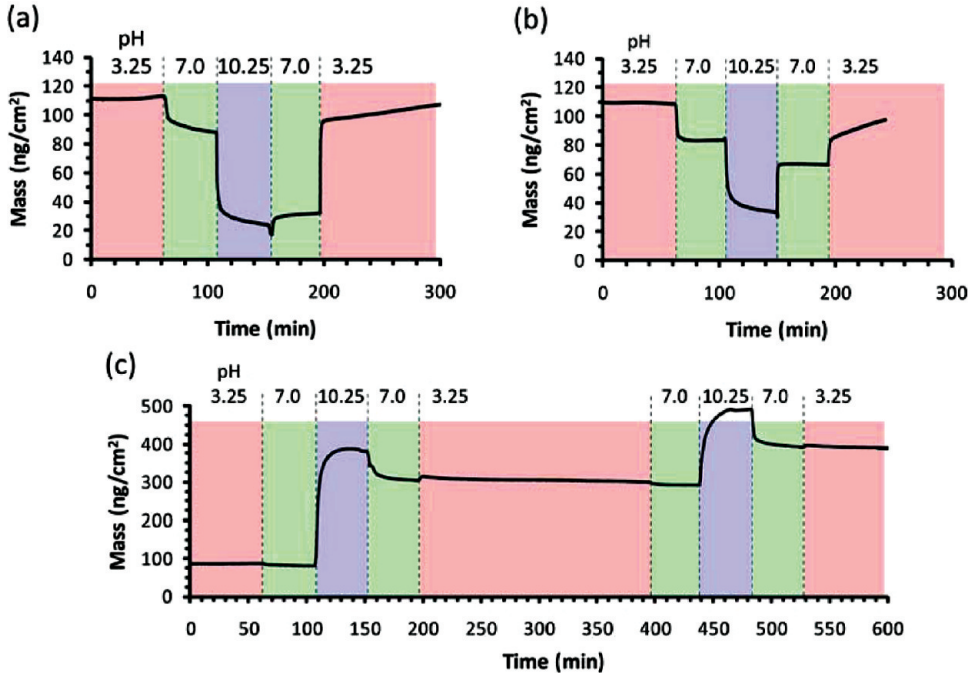

Figure 2. Areal mass density changes in 10-bilayer PAH/PSS films assembled at pH 9.5 as a function pH as measured by quartz crystal microbalance. (a) Unmodified PEM film, minimal ionic strength in the immersions. (b) Unmodified PEM film, 10 mM buffer solutions. (c) Acetic anhydride passivated PEM film, high ionic strength (10 mM buffers). The unmodified film shows the expected hysteresis versus pH, whereas the passivated film displays irreversible swelling at high pH values.

Gold Nanosphere Synthesis and Adsorption. Negatively charged, citrate-terminated gold nanoparticles were synthesized with the Turkevitch method.[36] This is the oldest and simplest method for making gold nanoparticles, and yields spheroidal particles with a fairly uniform size distribution. Briefly, 15 mg $HAuCl_4 \cdot 3H_2O$ was dissolved in 150 mL DI water and brought to a vigorous boil; 2.25 mL of a 10 mg/mL aqueous solution of trisodium citrate was then added as quickly as possible. The reaction was allowed to proceed for at least 5 min, and the resulting nanoparticle suspension was removed from the heat. After synthesis, the particles were cleaned three times with centrifugation and resuspension in DI water, which resulted in a ζ-potential of approximately −40 mV at a pH of about 5. The average diameter is largely determined by the ratio of citrate to gold salt. In our case, the average nanoparticle diameter is approximately 25 nm.

The negative charge of the gold nanospheres should cause them to adhere strongly to positively charged PEM surfaces, so surface adsorption of these particles was used as a simple way to visualize the adhesive properties of the PEM films and other substrates. This was done by simply immersing substrates in the nanosphere suspension for 3 h, after which the substrate was thoroughly rinsed with water and dried before imaging with scanning electron microscopy.

Nanosphere Lithography. A close-packed monolayer of polystyrene nanospheres was formed on the substrates from their suspension using convective self-assembly. The details of our method have been described elsewhere,[37] and largely follow the processes of Dimitrov and Nagayama[38] and Prevo and Velev.[39] Briefly, it involves placing a suspension of nanospheres at the inside corner of the space formed by the substrate surface and an angled plate suspended just above it. As the substrate is withdrawn horizontally at the correct speed, a monolayer colloidal crystal of close-packed polystyrene spheres forms at the receding contact line between the suspension droplet and the substrate. In most cases, we used positively charged amidine functionalized spheres, as the substrate surfaces were positively charged, and the technique requires that substrate and spheres have the same charge so that premature binding to the surface does not occur. 40 nm of gold or 30 nm of aluminum was then deposited onto the slides using electron beam evaporation. Most of the metal is blocked by the spheres, reaching the surface only through the triangular gaps between the spheres, after which the spheres were removed with adhesive tape, leaving behind an array of triangular particles. See Figure 6 below for representative micrographs.

RESULTS AND DISCUSSION

Amine-Rich PEMs. PEM (polyelectrolyte multilayer) films are a form of LbL films made by alternately applying positively and negatively charged polyelectrolytes to a surface from solution. In each deposition step, a polyelectrolyte is attracted and irreversibly bound to an oppositely charged surface. Deposition continues until there are no further sites where the polymer can bind, at which point the surface charge is reversed and deposition self-terminates. The process is then repeated with the oppositely charged polyelectrolyte. These steps can be repeated as many times as desired to build up a film of arbitrary thickness, which can be controlled with subnanometer precision.[20] Because each deposition step reverses the film charge, the film will contain approximately the same number of cations and anions, many of which are closely coordinated with each other in the film.

The particular type of PEM that interests us is made with amine-containing cations, specifically PAH (polyallylamine hydrochloride), and are assembled at pH $\gtrsim$8. The solution pK_a of PAH is 8.8, so this means that a large fraction of the amine groups in the PAH are unprotonated (and therefore charge neutral) during assembly, resulting in a film with a surplus of amines. Many amine groups are then free rather than coordinated with anions, as would be the case for films assembled at neutral pH. These films were pioneered by Rubner et al.,[19,40−42] and can be made from a variety of polymers; in addition to PAH, we use poly(styrene sulfonate) (PSS) as the anion. The uncoordinated amines make the films strongly adhesive to a wide variety of materials and molecules, including the gold nanoparticles we have used here to evaluate the adhesive properties of the film. It is also easy to couple a

variety of organic molecules and peptides to the amines,[14] so the surface properties of the film are easily modified.

Amine-rich PEM films have the remarkable property that they can undergo dramatic reversible swelling and deswelling as a function of pH.[40,41] Lowering ambient pH to ~3 causes the film to swell, gaining up to several hundred percent in thickness. The film can be returned to its original thickness if the pH is raised as high as 10. The hysteresis is due to coiling of the free amine groups into tightly packed hydrophobic domains at high pH. The pK_a of the amines in this state is quite low (~4),[41] so that strongly acidic conditions are required to reprotonate the amines. It is this protonation that causes the film to swell, as the charged amines repel each other and become screened by ions in the solvent. In the swelled film, the pK_a of the amines is at or above[41,43] their value in solution (~8.8), so deprotonation requires the pH to be raised above this value.

The hysteresis is thus a characteristic of amine-rich PEM films, and should go hand-in-hand with high adhesiveness also caused by the amines. The swelling as measured by quartz crystal microbalance (QCM) is shown in Figure 2. The QCM is capable of measuring changes in areal mass density of a film with precision in the ng/cm^2 range. The film was a $(PAH/PSS)_{10}$ film prepared at pH 9.5, the highest pH at which such a film can be prepared while still possessing good structural integrity. In each of the studied cases, the pH was allowed to equilibrate at a starting pH of 3.25. The pH was then changed to 7.0, 10.25, 7.0, and finally back to 3.25. This cycles the film through its full swell/deswell cycle. Panels a and b in Figure 2 both plot the results from the same film, with the distinction that in Figure 2a, the film was exposed to DI water where the pH had been adjusted by minimal addition of HCl or NaOH, whereas in Figure 2b, the films were exposed to buffered solutions (standard 10 mM solutions of citrate buffer, phosphate buffered saline, and carbonate buffer for pH 3.25, 7.0, and 10.25 respectively). In both cases, the expected swelling (deswelling) is observed at low (high) pH as a change in the areal density of the film. The expected hysteresis is observed at pH 7, although it is smaller if the film is exposed to buffers rather than pH adjusted DI water. This suggests that the degree of swelling in the film and thereby the degree of amine protonation and adhesiveness can be tuned continuously by both the pH history and the ionic strength of the solution in which it is immersed.

The effect of the same sequence of pH values on an anhydride-treated PEM film is plotted in Figure 2c. The acetic anhydride reacts with the amines, transforming them into neutral amides, which should not contribute to adhesion to the film. In this case, low pH values do not affect the film appreciably, but exposure to high pH causes the film to swell. A likely explanation for this is that only a small number of unreacted amines remain in the film, and when a large fraction of these are deprotonated, much of the electrostatic attraction that holds the film together is removed, allowing water to infiltrate it. Some of this water remains in the film when the pH is returned to neutral or lower pH, so the swelling is partially irreversible.

One possible use of the hysteresis is for regulation of the quantity of amines available at the surface near neutral pH, which should make it possible to adjust the degree of adhesion to the film. However, we find that adhesion is quite strong even when adsorbing onto a deswelled film, thus this possibility is not investigated further here. Perhaps more interestingly, the ability to adjust film thickness means one can adjust the effective index of refraction seen by nanostructures attached to the film as well as the separation between the nanostructures and the substrate, which would provide a way to tune plasmon resonances and other optical properties after surface fixation.[44,45]

Because the swelling and deswelling processes involve coiling and uncoiling of amine groups into hydrophobic domains, it necessarily entails some rearrangement of the polymer molecules in the film. This is consistent with observations by Itano et al.,[41] who noted a large increase in film roughness with successive swell/deswell cycles as measured by AFM. We observe the same phenomenon in SEM images of a $(PAH/PSS)_{10}/PAH$ film prepared at pH 9.5 (Figure 3) where the roughness of the film clearly increases with the number of swell/deswell cycles. We posit that this rearrangement is an important factor in maintaining adhesiveness of the film after lithographic processing, and we present direct evidence of this in a later section.

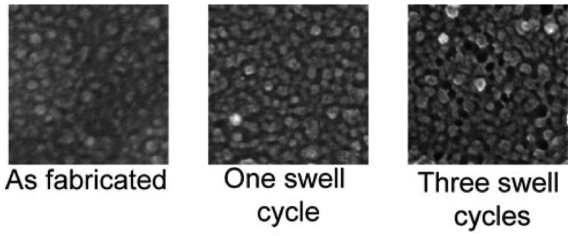

Figure 3. SEM images of an amine-rich PEM film as it undergoes repeated swell/deswell cycles. All micrographs are taken with the same settings, so the increase in contrast with processing reflects a real roughening of the surface, including the appearance of nanopores in the film after three cycles. Each image is 400 nm on a side.

Adhesion Patterning with a Metallic Mask. When amine-rich PEM films are immersed in a suspension of negatively charged gold nanoparticles, the particles adsorb readily on the surface, as expected. The films can be well-approximated as perfect adsorbing collectors, where every particle that comes within some small distance of the surface sticks irreversibly. This process is well-understood[46,47] and will not be discussed further here. We are instead interested in patterning the particle adhesion to the surface, and this requires the amine content of the surface to be modulated. We elected to do this with acetic anhydride, which converts most of the film's amines into amides. To create a pattern, areas where we wished to retain the adhesive properties were protected with a 30 nm thick layer of aluminum which was etched away after the acetic anhydride treatment. For demonstration purposes, the surface was patterned by evaporating the aluminum through a 200 mesh TEM grid that was attached to the substrate, resulting in an array of aluminum squares, each 85 μm across. The substrate was then treated with acetic anhydride as described in the experimental section. The aluminum was removed by etching in a 1 mM (pH 3.0), 45 °C solution of HCl for 45 min. The pH of the etch solution causes the film to swell, and while it is possible to adsorb particles onto the substrate at this stage, for consistency's sake we chose to always perform the adsorption on the film in the deswelled state. Therefore, the film was exposed to pH 10.25 for 30 min before being immersed in a gold particle suspension for 1 h.

When this process is applied to a $(PAH/PSS)_n/PAH$ film prepared at pH 9.5, it results in a dense coverage of gold nanoparticles in the areas that were protected by aluminum, with a much sparser coverage in regions treated with acetic anhydride, as shown in Figure 4. For the particular deposition

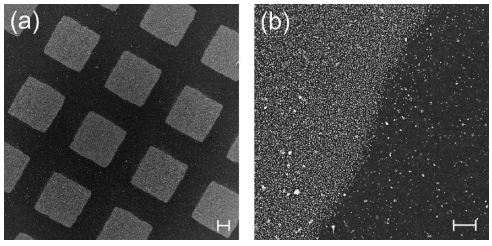

Figure 4. SEM micrographs of an adhesion-patterned amine-rich PEM prepared at pH 9.5, with gold nanoparticles (light shade) adsorbed to visualize the adhesion. The lengths of the scalebars are (a) 20 μm and (b) 1 μm.

conditions used here, we count approximately 115 particles/μm^2 in the protected regions versus less than 5 particles/μm^2 in the treated areas.

The nanoparticles adhered to the surface exhibit the expected resonance near 530 nm wavelength, which manifests as an increase in scattering and absorption of light, as shown in Figure 5. The micrograph inset in the figure is taken with a

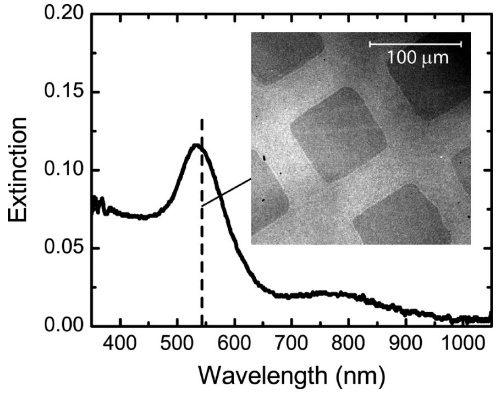

Figure 5. Plot of the extinction (absorption + scattering) spectrum for light transmitted through an adhesion-patterned sample with adsorbed gold nanoparticles, showing the characteristic peak near 530 nm. The inset shows an image of reflected 543 nm light from a green HeNe laser (wavelength indicated by the vertical dashed line) taken with a confocal microscope. The areas coated with gold particles appear darker due to the strong scattering of the laser light in those regions.

Zeiss LSM510 confocal microscope and shows the reflectance of a green HeNe laser (wavelength 543 nm) off the surface. Because the laser is resonant with the plasmon modes of the gold spheres, it is scattered strongly by those areas where the particles are adsorbed, which consequently appear darker in the image.

The process just described enables us to pattern the adhesiveness of the surface into arbitrary patterns, after which particles, proteins or small molecules can beadsorbed onto the surface as desired. Since this is the last step, no constraints are placed on the adsorbate other than the ability to bind to the surface of the film, and particles and molecules that are incompatible with the lithographic process can thus be deposited in a simple manner. The spatial resolution also appears to be quite good, and certainly no worse than 300 nm. But for a better test of the resolution capability, we need to turn to a lithographic technique capable of higher resolution.

Nanosphere Lithography for High-Resolution Adhesion Patterning of Amine-Rich PEM Films. Nanosphere lithography (NSL)[48] is one of the simplest ways to fabricate nanostructures on a surface, and it is our choice for testing the resolution limit of the adhesion patterning just described. As mentioned in the experimental section, NSL relies on our ability to make polystyrene nanospheres that are a few hundred nanometers in diameter pack into a single closepacked monolayer on the surface, as shown in the micrograph in Figure 6a. When this is accomplished, metal evaporated onto

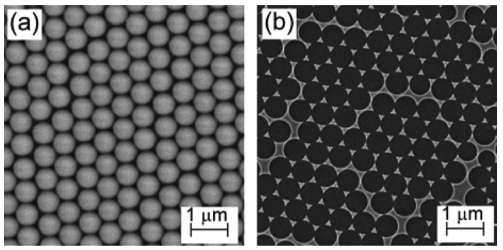

Figure 6. SEM micrographs of (a) a closepacked monolayer of polystyrene nanospheres assembled with convective self-assembly, and (b) the array of triangular nanoparticles that results when metal is evaporated onto the polystyrenes spheres, which are then removed.

the sample will reach the substrate through the triangular spaces between the spheres, resulting in arrays of triangular particles that are revealed when the spheres are removed, as shown in Figure 6b. The particle arrays can cover large areas, as much as several cm^2. The particles also have very sharp corners, with radii down to 10 nm or less, which makes them particularly suitable for plasmonic applications such as surface enhanced Raman spectroscopy.[30]

The quality of the NSL is highly dependent on surface properties, and can in fact only be performed if there is no significant adhesion between the surface and the polystyrene nanospheres while they assemble into a colloidal crystal. To minimize the surface adhesion, we used positively charged amidine-terminated nanospheres, and ensure that the PEM film is in its deswelled state. Figure 7a–d show optical micrographs of polystyrene colloidal crystals (similar to Figure 6a, but at lower resolution) assembled with convective self-assembly on amine-rich PEM films of varying thickness. Each white disk corresponds to a polystyrene nanosphere, and defects in the crystal structure of the closepacked layer appear as dark spots and lines. For comparison purposes, we also deposited colloidal crystals on a substrate coated with aminopropyltriethoxysilane (APTES) (Figure 7e) and directly on glass (Figure 7f). Treating a glass substrate with APTES results in a surface functionalized with amines, and is a standard technique in cell biology and related fields.[49−51] Because glass is negatively charged in neutral aqueous solutions, negatively charged carboxyl-terminated polystyrene nanospheres were used for NSL on the untreated glass surface. All crystals were fabricated on the same day, and at the same ambient temperature and humidity. The crystal defect density can therefore serve as a rough indicator of the propensity of the surface to bind the polystyrene nanoparticles during the deposition process.

The colloidal crystal quality is unquestionably the highest on the glass substrate. Only a few vacancies are seen and the vast

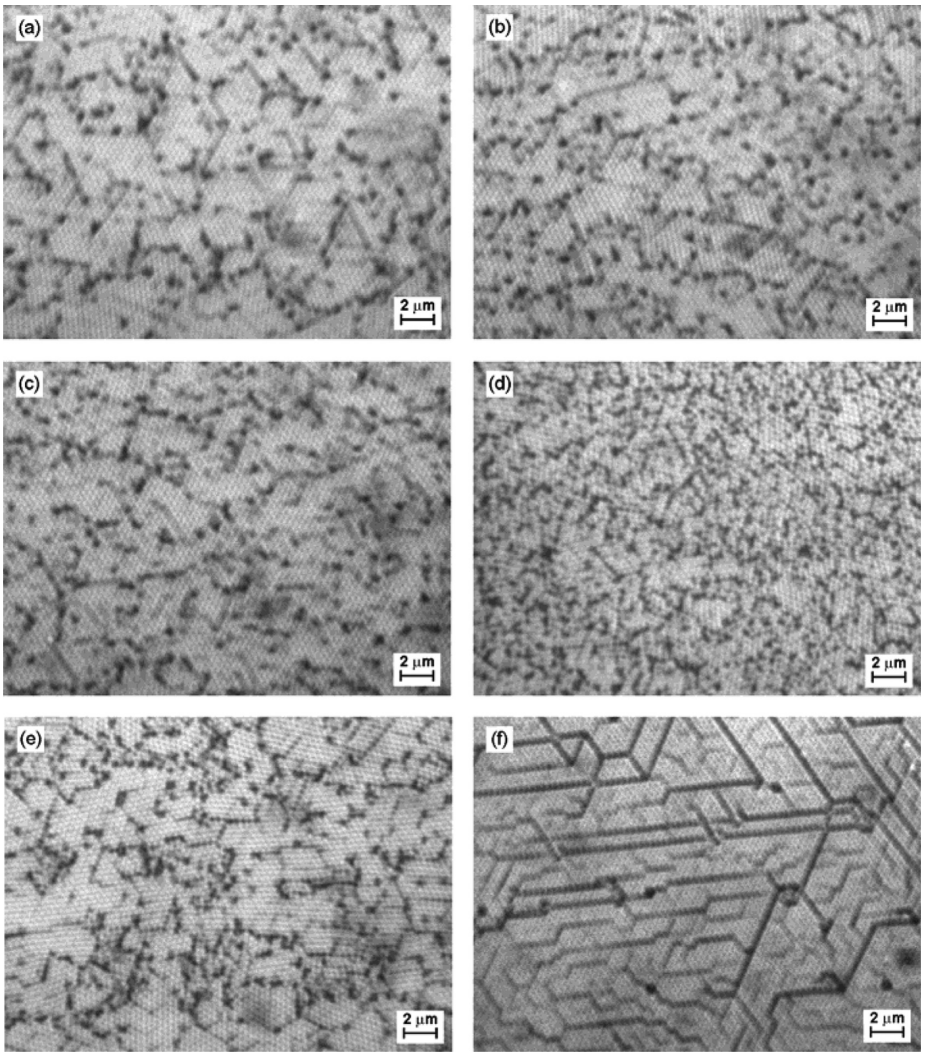

Figure 7. Optical micrographs of colloidal crystals of polystyrene nanospheres deposited with nanosphere lithography, illustrating the dependence of colloidal crystal domain size on the substrate. The spheres are visible as small white disks arranged in a hexagonal close-packed pattern. Defects and missing spheres in the colloidal crystal show up as dark lines and spots. (a) Colloidal crystals deposited on: PAH/PSS/PAH film deposited at pH 9.5. (b) $(PAH/PSS)_2$/PAH film. (c) $(PAH/PSS)_5$/PAH film. (d) $(PAH/PSS)_{10}$/PAH film. (e) APTES-terminated substrate. (f) Unadorned glass. Positively charged amidine-terminated spheres were used in samples a–e, and negatively charged carboxyl-terminated spheres were used in sample f. Both types of particles were 450 nm in diameter.

majority of defects are line defects that occur due to imperfections in the sphere packing. On the amine terminated surfaces there are numerous vacancies, indicating a greater propensity for the particles to stick to the surface rather than packing into an ordered monolayer. This effect also leads to smaller crystalline domains and less long-range order in the crystal. In spite of this, the quality of the crystal is sufficient for our purposes, as metal deposition onto the crystals will result in a majority of triangular particles in all cases. In the PEM films, the defect density increases with increasing film thickness, likely due to greater roughness in the thicker films. The defect density seen in the 2-bilayer sample is roughly equivalent to what is seen in the APTES sample, and the two are largely equivalent from the point of view of the convective self-assembly process. However, the APTES sample suffers from a lack of uniformity, which means that a monolayer colloidal crystal forms only over some fraction of the surface, whereas it is straightforward to deposit such a layer over the entire PEM film substrate.

When gold nanotriangles are deposited directly on glass with NSL, the adhesion is insufficient to keep them in place even when exposed to a fairly mild disturbance. For instance, adsorbing a monolayer of dodecanethiol onto the particles will lift them off the surface, as is seen in Figure 8a. If the substrate is coated with an amine-rich PEM film before the NSL, the particles are fixed in place, and will not lift off after thiol treatment or brief ultrasonication. At this point, the surface between the nanoparticles remains highly adhesive, and readily adsorbs gold nanospheres, as is shown in Figure 8b. Not unexpectedly, the adsorption of gold spheres can be prevented by first passivating the surface with acetic anhydride. The areas of the film already covered by triangular particles is not affected by this, so the triangular particles remain strongly attached to the film, even though the acetic anhydride has suppressed adsorption of gold nanospheres in the areas between the particles, as can be seen in Figure 8c.

To use NSL for adhesion patterning, nanotriangles made of aluminum were used, and the substrate was passivated, etched, and deswelled as described above. Electron micrographs of the substrate before (Figure 9a) and after (Figure 9b) this treatment are shown in Figure 9, where nanospheres adsorb

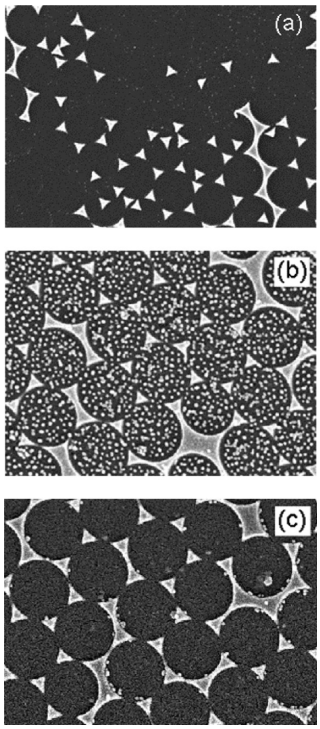

Figure 8. SEM micrographs of gold nanotriangles deposited with nanosphere lithography on different substrates; (a) directly on glass, showing poor adhesion after deposition of dodecanethiol; (b) on an amine-rich PSS/PAH film, with gold nanospheres adsorbed in a second step; and (c) on a PEM film that was then treated with acetic anhydride and onto which gold nanospheres were then adsorbed.

densely on the parts of the surface that were protected by the triangular particles, with very little adsorption onto areas that have seen direct exposure to acetic anhydride. The spatial resolution of this process is very good, demonstrably better than 100 nm.

pH Cycling and Surface Adhesion. We have already seen that when an amine-rich PEM is taken through a swell/deswell cycle, this leads to a significant rearrangement of the material in the film, producing a new configuration of the surface.[41] Our hypothesis is that this lends a great deal of robustness to the adhesive properties of the films, which are left unchanged even by significant damage and fouling of the surface. This would explain how the films remain adhesive even after such harsh and potentially disruptive a process as metal evaporation.

The process can work this way even if there is little or no vertical intermixing in the film during a swell/deswell cycle, and even if only a fraction of the surface is rejuvenated. It is quite sufficient that a rearrangement of the topmost polymer molecules leads to formation of a network of positively charged virgin amine-rich patches on the surface of the film. For example, Kozlova et al.[52] demonstrated that such patches, covering as little as 20% of a surface, can make the surface just as adhesive to oppositely charged particles as if it were uniformly charged. Kalasin et al.[53] showed that a coarsening rearrangement in surface functionalization can cause a substrate to go from being nonadhesive to strongly adhesive, even when no functional groups are added to or removed from the surface.

To verify the rejuvenation hypothesis, we fabricated $(PAH/PSS)_{10}$ films at pH 9.5, which were exposed to different pretreatments before adsorption of negatively charged gold nanoparticles onto the surface was attempted. The top PSS

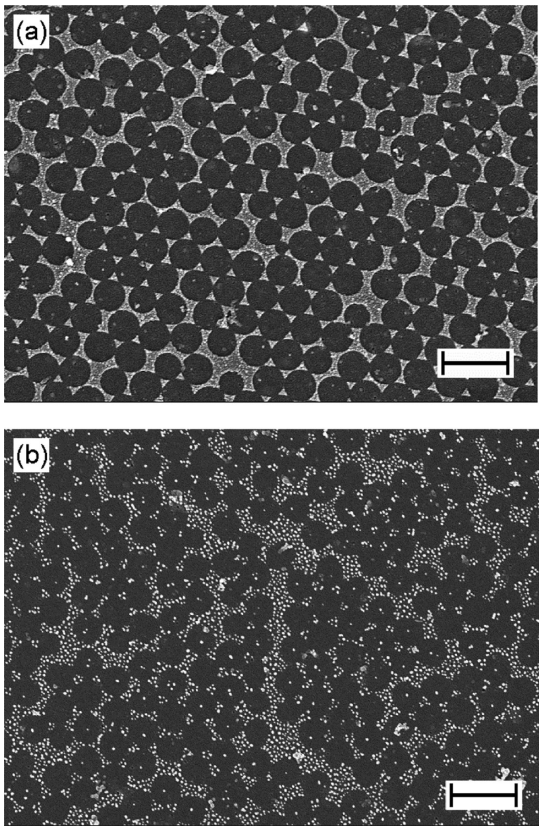

Figure 9. (a) Micrograph of a PEM film with Al nanoparticles applied using nanosphere lithography. (b) The same film after passivation with acetic anhydride, wet etch removal of Al particles, and adsorption of gold nanoparticles. The scales bar are 1 μm.

layers made the surfaces negatively charged so that gold nanoparticles do not adsorb, similarly to how surface damage or fouling could be expected to diminish the adsorptivity of a PAH terminated film. This is clear from Figure 10a, where few

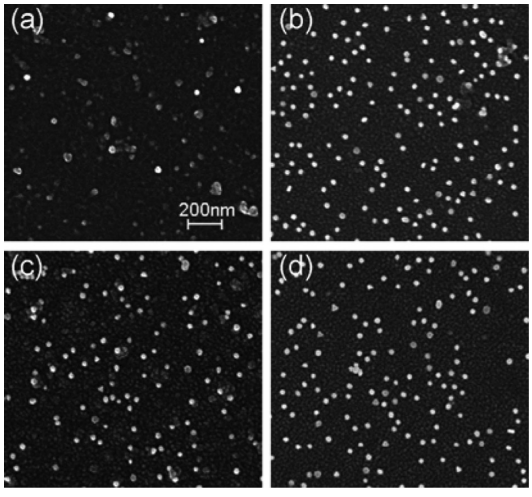

Figure 10. Gold nanosphere adsorbed onto an amine-rich PEM terminated with a layer of anionic PSS. (a) As first prepared, very few particles adsorb on the film. (b) Particle adsorption is good after the film has been swelled by immersion in a low pH solution. (c) Adsorption remains good after the swelled film has been reduced to its original thickness by immersion in a high pH solution. (d) The film remains strongly adhesive after three full swell/deswell cycles.

particles have adsorbed onto the film when the freshly fabricated film was immersed into a nanoparticle suspension with only an intervening rapid rinse in DI water. If the film is swelled before rinsing, particles adsorb readily on the surface (Figure 10b). This is expected, because the low pH protonates many of the amines that were initially neutral, giving the film a positive surface charge. If, by contrast, the films is put through a full swell/deswell cycle before particle adsorption is carried out, the degree of protonation in the amines will be similar to when the film was first fabricated. In spite of this, particles readily adsorb onto a $(PAH/PSS)_{10}$ film that has been through one (Figure 10c) or multiple (Figure 10d) swell/deswell cycles.

Itano et al.[41] showed that the fraction of PAH in these films increases with preparation pH. We verified that this applies to our films by quantifying the fraction of nitrogen and sulfur in the films with XPS. The results are shown in Figure 11. We

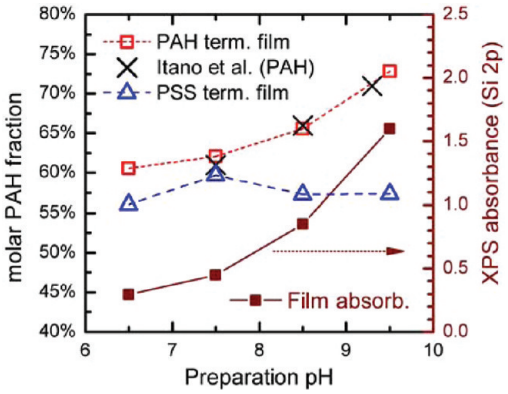

Figure 11. Fraction of PAH in PAH/PSS films as determined by XPS for $(PAH/PSS)_5/PAH$ (empty red squares) and $(PAH/PSS)_5$ films (empty blue triangles) compared to the values reported by Itano et al.[41] (black X's). The filled squares indicated the absorbance of the films at the Si 2p XPS line.

tested both $(PAH/PSS)_5/PAH$ and $(PAH/PSS)_5$ films, prepared at pH values of 6.5, 7.5, 8.5, and 9.5. Our results are in good agreement with previous reports[41] for both PAH-terminated films and PSS-terminated films (the latter not shown). There is, however, some discrepancy between the two film types, in that XPS on PSS-terminated films yield lower observed PAH-fractions both for high and low preparation pH. To explain this, Figure 11 also plots the absorbance A of the Si 2p XPS line, defined as $A = \log_{10}(I^{Si\ 2p}_{blank}/I^{Si\ 2p}_{film})$, where $I^{Si\ 2p}_{blank}$ and $I^{Si\ 2p}_{film}$ are the XPS signals for the Si 2p lines for blank and film-covered substrates respectively. Because the Si signal comes from the SiO_2 substrate, this is a measure of the attenuation of the XPS photoelectrons as they traverse the film, and hence also an indication of the surface mass density. At high preparation pH, the films become substantially thicker, and the topmost polyelectrolyte layer therefore comes to dominate the XPS signal, which explains the difference between PSS and PAH-terminated films at high preparation pH. At pH 6.5, the film is thin enough that all layers provide a similar contribution to the XPS signal. Since the $(PAH/PSS)_5/PAH$ films contain about 20% more PAH than the $(PAH/PSS)_5$ film, this explains the difference between the two film types observed at this preparation pH. At pH 7.5, the film is thick enough that the difference in total quantities of PAH and PSS in the film has a small effect on the measurement, while each individual monolayer is thin enough that that it is of little importance which polymer was deposited last. As a result, the observed difference between the two film types is the smallest at this pH.

Because the films prepared at the largest pH have the highest fraction of amine groups, we expect them to exhibit the strongest adhesion. To test this, we prepared $(PAH/PSS)_{10}/PAH$ films at pH values of 6.5, 7.5, 8.5, and 9.5. Two samples were made at each pH, one of which was passivated with acetic anhydride while the other was left as fabricated. These eight films were all immersed in a gold particle suspension, and were then imaged with SEM to determine the surface particle density. The results are plotted in Figure 12, where there is a

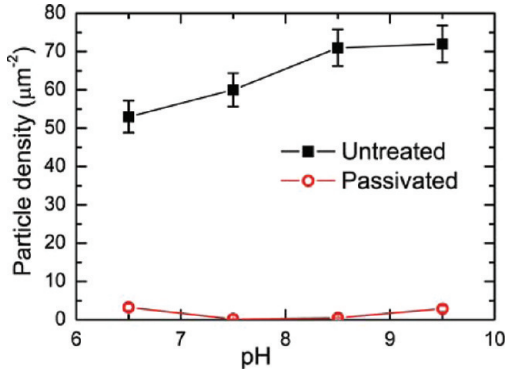

Figure 12. Plot of the density of adsorbed nanoparticles on amine-rich PEM films as a function of preparation pH and post-treatment. In untreated films, the particle density increases with the excess of amines in the film.

clear trend toward better adsorptivity in unpassivated films prepared at higher pH, correlating with a the higher fraction of uncoordinated amine groups in these films. Films passivated with acetic anhydride show very little binding, as expected.

We also tested the robustness of the adhesive properties in films prepared at different pH values. Each film was patterned by aluminum evaporation through a TEM grid and exposed to acetic anhydride for 20 min. The Al mask was etched away with dilute HCl and the films were deswelled at pH 10.25 before gold nanoparticles were introduced. Figure 13 shows micrographs of these films, prepared at pH 7.5, 8.5, and 9.5. It is clear that that the higher the pH at which the film was prepared, the better the adhesion of particles to the film. The film prepared at pH 9.5 shows uniform attachment of spheres across the surface that has been protected from acetic anhydride. Films prepared at the lower pH values show good adhesion except in patches that surround polyp-like protrusion from the film. Presumably, these protrusions contain material that was displaced from the rest of the film during the swell/deswell process. We then expect surface rejuvenation to be less complete the shorter the distance to the protrusion, which explains the observed patches.

We observe the effects of surface rejuvenation in films fabricated at pH 7.5, even though pH cycling does not lead to detectable thickness changes in such films.[41] The degree of ionization in dissolved PAH at pH 7.5 is >80%, so that PSS/PAH films prepared at this pH contain close to the same number of cations as anions, which coordinate with each other, precluding the formation of amine-rich domains.

However, surface and bulk properties do not have to behave identically, so a lack of swelling in the film as a whole does not preclude significant pH-induced structural changes in the top layer. To examine this more quantitatively, we measured the streaming potential in several PAH/PSS films. The streaming

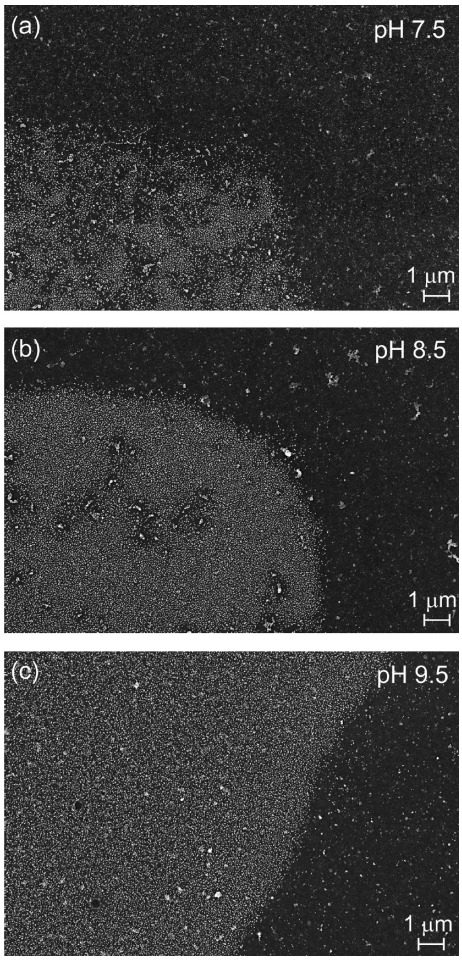

Figure 13. SEM micrographs of adhesion-patterned PEM films prepared at different pH values, with gold nanoparticles used to visualize the adhesion. The uniformity of the adhesion is better the higher the preparation pH of the film.

potential is a measure of the average surface potential, akin to the zeta-potential in colloids, but measured over extended surfaces. For the experiment, four $(PAH/PSS)_{10}$ films were prepared at pH 6.5, 7.5, 8.5, and 9.5. The streaming potential was then measured as the pH was cycled between 3.25 and 10.25. The results are plotted in Figure 14. As expected, all the films carry a negative charge at high pH and a positive charge at low pH. Near neutral conditions, the films prepared at pH 7.5 and higher exhibit a distinct hysteresis in the surface potential as the pH is cycled up and down. This is consistent with formation of hydrophobic amine-rich domains at high pH. The film prepared at pH 6.5 is contains little excess of amines, and consequently shows no hysteresis.

CONCLUSION

We have shown that amine-rich PSS/PAH polyelectrolyte multilayer films are an excellent choice for surface adhesion of metal nanostructures. Fabrication of the films is straightforward, and does not involve any toxic chemicals, and a film with highly uniform properties is readily obtained.

The surface adhesion can be passivated with acetic anhydride without affecting the binding of structures already attached to the surface. This is particularly useful since it may allow nanoassembly to be performed on a surface without encountering unwanted nonspecific surface binding. Arbitrary

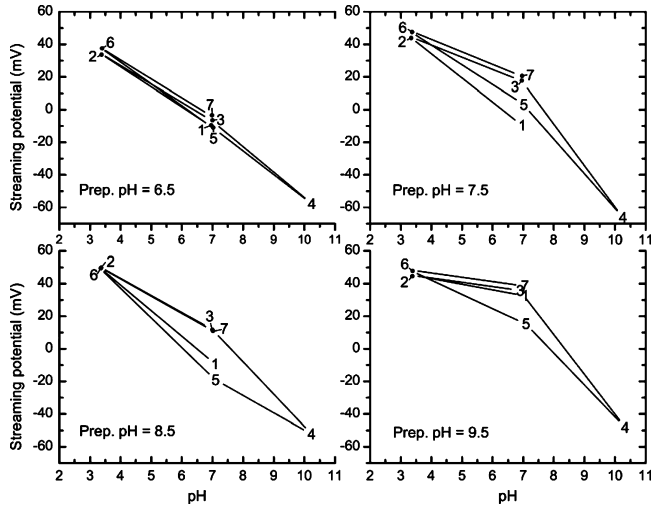

Figure 14. Streaming potential measurements in PEM films with different preparation pH. The numbers 1−7 in each panel represent the order of exposure to high, low, and neutral pH. Hysteresis is seen in the films where there is excess of amine groups as the conformation of the film at neutral pH varies by pH history. The film prepared at pH 6.5 has few excess amines, and accordingly, no hysteresis is seen.

patterns of adhesiveness can be readily fabricated by taking advantage of this property, protecting areas where adhesiveness is to be retained with an evaporated aluminum mask that is removable with chemical wet etching.

This process can be used to direct assembly of nanostructures to particular areas, which is of great importance when bottom-up fabricated nanostructures are to be integrated into larger devices or systems. On the life science side, similar requirements arise in areas such as tissue engineering, and the fact that no postprocessing is required after the adhesion step is particularly useful when working with living cells or other structures that cannot withstand the processing conditions of standard lithography. As the films are easy to fabricate with high uniformity and repeatability, they could also potentially be used as a replacement for standard APTES-terminated substrates.

We hypothesize that the ability to pattern the adhesiveness of these films with a rather harsh lithographic process arises from the dynamical nature of their conformation. The adhesion comes from uncoordinated amine groups which exist at all levels or the film, and which mostly are protected in coiled-up hydrophobic domains. Cycling the pH reorganizes the film, exposing virgin amine groups on the surface, and removing damage caused by the metal evaporation and subsequent etch.

Finally, we note that nanosphere lithography, relying on convective self-assembly of polystyrene nanospheres to form a template for metal evaporation, can readily be performed on the films. It results in a large number of triangular nanoparticles, even if the colloidal crystal template has a significantly higher defect density compared to what is seen in convective self-assembly on plain glass.

AUTHOR INFORMATION

Corresponding Author

*hansr@vt.edu.

Notes

The authors declare no competing financial interest.

■ ACKNOWLEDGMENTS

The authors gratefully acknowledge Dr. Richey M. Davis for fruitful discussions and for use of the Q-Sense E4 quartz crystal microbalance, and Dr. John Y. Walz for use of the Anton-Paar SurPASS electrokinetic analyzer. This work was supported by the Institute of Critical Technology and Applied Science (ICTAS), a grant from the National Science Foundation (Agreement DMR-1006753), and by a grant from the Thomas F. Jeffress and Kate Miller Jeffress Memorial Trust.

■ REFERENCES

(1) Sau, T. K.; Rogach, A. L. *Adv. Mater.* **2010**, *22*, 1781−1804.
(2) Pal, S.; Deng, Z. T.; Ding, B. Q.; Yan, H.; Liu, Y. *Angew. Chem., Int. Ed.* **2010**, *49*, 2700−2704.
(3) Fava, D.; Nie, Z.; Winnik, M. A.; Kumacheva, E. *Adv. Mater.* **2008**, *20*, 4318−4322.
(4) Hong, L.; Cacciuto, A.; Luijten, E.; Granick, S. *Nano Lett.* **2006**, *6*, 2510−2514.
(5) Caswell, K. K.; Wilson, J. N.; Bunz, U. H. F.; Murphy, C. J. *J. Am. Chem. Soc.* **2003**, *125*, 13914−13915.
(6) Yap, F. L.; Zhang, Y. *Biosens. Bioelectron.* **2007**, *22*, 775−788.
(7) Veiseh, M.; Zareie, M. H.; Zhang, M. Q. *Langmuir* **2002**, *18*, 6671−6678.
(8) Mohammed, J. S.; DeCoster, M. A.; McShane, M. J. *Biomacromolecules* **2004**, *5*, 1745−1755.
(9) Jung, J. Y.; Kim, K. W.; Na, K.; Kaholek, M.; Zauscher, S.; Hyun, J. *Macromol. Rapid Commun.* **2006**, *27*, 776−780.
(10) Zheng, H. P.; Berg, M. C.; Rubner, M. F.; Hammond, P. T. *Langmuir* **2004**, *20*, 7215−7222.
(11) Ai, H.; Lvov, Y. M.; Mills, D. K.; Jennings, M.; Alexander, J. S.; Jones, S. A. *Cell Biochem. Biophys.* **2003**, *38*, 103−114.
(12) Lyles, B. F.; Terrot, M. S.; Hammond, P. T.; Gast, A. P. *Langmuir* **2004**, *20*, 3028−3031.
(13) Lee, K. B.; Lim, J. H.; Mirkin, C. A. *J. Am. Chem. Soc.* **2003**, *125*, 5588−5589.
(14) Reyes, D. R.; Perruccio, E. M.; Becerra, S. P.; Locascio, L. E.; Gaitan, M. *Langmuir* **2004**, *20*, 8805−8811.
(15) Winkleman, A.; Gates, B. D.; McCarty, L. S.; Whitesides, G. M. *Adv. Mater.* **2005**, *17*, 1507−1511.
(16) Suzuki, M.; Yasukawa, T.; Mase, Y.; Oyamatsu, D.; Shiku, H.; Matsue, T. *Langmuir* **2004**, *20*, 11005−11011.
(17) Kimura, T.; Sato, Y.; Kimura, F.; Iwasaka, M.; Ueno, S. *Langmuir* **2005**, *21*, 830−832.
(18) Bertrand, P.; Jonas, A.; Laschewsky, A.; Legras, R. *Macromol. Rapid Commun.* **2000**, *21*, 319−348.
(19) Rubner, M. F., pH-Controlled Fabrication of Polyelectrolyte Multilayers: Assembly and Applications. In *Multilayer Thin Films*, Decher, G.; Schlenoff, J. B., Eds. Wiley: 2003; pp 133−154.
(20) Decher, G.; Hong, J. D.; Schmitt, J. *Thin Solid Films* **1992**, *210*−*211*, 831−835.
(21) Park, J.; Fouche, L. D.; Hammond, P. T. *Adv. Mater.* **2005**, *17*, 2575−2579.
(22) Cho, C. Y.; Valverde, L.; Ozin, G. A.; Zacharia, N. S. *Langmuir* **2010**, *26*, 13637−13643.
(23) Park, J.; Hammond, P. T. *Adv. Mater.* **2004**, *16*, 520−525.
(24) Kidambi, S.; Chan, C.; Lee, I. *J. Am. Chem. Soc.* **2004**, *126*, 4697−4703.
(25) Zhang, C.; Hirt, D. E. *Polymer* **2007**, *48*, 6748−6754.
(26) Mitsui, K.; Handa, Y.; Kajikawa, K. *Appl. Phys. Lett.* **2004**, *85*, 4231−4233.
(27) Nath, N.; Chilkoti, A. *Anal. Chem.* **2002**, *74*, 504−509.
(28) Cheng, S. F.; Chau, L. K. *Anal. Chem.* **2003**, *75*, 16−21.
(29) Zhao, J.; Zhang, X.; Yonzon, C. R.; Haes, A. J.; Van Duyne, R. P. *Nanomed.* **2006**, *1*, 219−228.
(30) Haynes, C. L.; Van Duyne, R. P. *J. Phys. Chem. B* **2003**, *107*, 7426−7433.
(31) Nie, S.; Emory, S. R. *Science* **1997**, *275*, 1102−1106.
(32) Kneipp, K.; Wang, Y.; Kneipp, H.; Perelman, L. T.; Itzkan, I.; Dasari, R.; Feld, M. S. *Phys. Rev. Lett.* **1997**, *78*, 1667−1670.
(33) Haes, A. J.; Hall, W. P.; Chang, L.; Klein, W. L.; Van Duyne, R. P. *Nano Lett.* **2004**, *4*, 1029−1034.
(34) Ekgasit, S.; Thammacharoen, C.; Yu, F.; Knoll, W. *Appl. Spectrosc.* **2005**, *59*, 661−667.
(35) Adamczyk, Z.; Jaszczolt, K.; Siwek, B.; Weronski, P. *Langmuir* **2005**, *21*, 8952−8959.
(36) Frens, G. *Nature Phys. Sci.* **1973**, *241*, 20−22.
(37) Chen, K.; Stoianov, S. V.; Bangerter, J.; Robinson, H. D. *J. Colloid Interface Sci.* **2010**, *344*, 315−320.
(38) Dimitrov, A. S.; Nagayama, K. *Langmuir* **1996**, *12*, 1303−1311.
(39) Prevo, B. G.; Velev, O. D. *Langmuir* **2004**, *20*, 2099−2107.
(40) Hiller, J.; Rubner, M. F. *Macromolecules* **2003**, *36*, 4078−4083.
(41) Itano, K.; Choi, J. Y.; Rubner, M. F. *Macromolecules* **2005**, *38*, 3450−3460.
(42) Hiller, J.; Mendelsohn, J. D.; Rubner, M. F. *Nat. Mater.* **2002**, *1*, 59−63.
(43) Burke, S. E.; Barrett, C. J. *Langmuir* **2003**, *19*, 3297−3303.
(44) Gupta, M. K.; Chang, S.; Singamaneni, S.; Drummy, L. F.; Gunawidjaja, R.; Naik, R. R.; Tsukruk, V. V. *Small* **2011**, *7*, 1192−1198.
(45) Nergiz, S. Z.; Singamaneni, S. *ACS Appl. Mat. Interfaces* **2011**, *3*, 945−951.
(46) Grabar, K. C.; Smith, P. C.; Musick, M. D.; Davis, J. A.; Walter, D. G.; Jackson, M. A.; Guthrie, A. P.; Natan, M. J. *J. Am. Chem. Soc.* **1996**, *118*, 1148−1153.
(47) Adamczyk, Z.; Jaszczolt, K.; Siwek, B.; Weronski, P. *J. Chem. Phys.* **2004**, *120*, 11155−11162.
(48) Haynes, C. L.; Van Duyne, R. P. *J. Phys. Chem. B* **2001**, *105*, 5599−5611.
(49) Sapsford, K. E.; Ligler, F. S. *Biosens. Bioelectron.* **2004**, *19*, 1045−1055.
(50) Nakagawa, T.; Tanaka, T.; Niwa, D.; Osaka, T.; Takeyama, H.; Matsunaga, T. *J. Biotechnol.* **2005**, *116*, 105−111.
(51) Howarter, J. A.; Youngblood, J. P. *Langmuir* **2006**, *22*, 11142−11147.
(52) Kozlova, N.; Santore, M. M. *Langmuir* **2006**, *22*, 1135−1142.
(53) Kalasin, S.; Martwiset, S.; Coughlin, E. B.; Santore, M. M. *Langmuir* **2010**, *26*, 16865−16870.